

Fitted Policy Iteration for a POMDP Peg-In-Hole search task.

Guillaume de Chambrier^{a,1,*}, Aude Billard^a

^a*Learning Algorithms and Systems Laboratory (LASA), École Polytechnique Fédérale de Lausanne (EPFL), Switzerland*

Abstract

A policy can be obtained by encoding the tasks as a partially observable markov decision process (POMDP) and then solve it by dynamic programming. This quickly become infeasible for relatively high-dimensional continuous tasks. To address this problem we demonstrate how human intuition can be leveraged to learn a belief space policy. A set of human teachers demonstrate the search PiH task during which the position uncertainty, represented by a Point Mass Filter (PMF), is recorded and compressed to the most likely state and entropy. A policy parametrised by a Gaussian Mixture Model (GMM) is learned and refined in an Actor-Critic Fitted reinforcement learning framework. We evaluate Actor-Critic policy, called Q-EM, against a Greedy and non-optimised GMM policy with respect to the distance taken to localise the socket and the distance taken to establish a connection between the plug and power socket. We test the ability of the learned models to generalise to different socket types and locations. We found that the Actor-Critic policy is always better in terms of distance travelled to localise the socket. We tested on a KUKA LWR robot, across three different power sockets, the ability of the Q-EM, GMM and Greedy policies to find and connect a plug to the power socket. We found when the socket has no distinctive features both data learned policy are better but when features are present the Greedy policy does just as good, or better.

Keywords: Fitted Reinforcement Learning, Actor-Critic, POMDP, GMM policy, Programming by Demonstration

1. Introduction

The ability to act optimally given uncertainty is paramount for robotic systems to be successful in environments which are not fully observable. Depending on the task and structure of the uncertainty, if not taken into consideration by the control policy, can lead to waist-full usage of resources and even fail to accomplish the task. Given the potential adverse (disastrous if considering a search and rescue task) consequences, it is important to design uncertainty robust policies and planners.

The generic solution to such an optimal control problem is to formulate the task as Partially Observable Markov Decision Process (POMDP) which is subsequently solved by dynamic programming or reinforcement learning if the transition and observation models are unavailable. It is well known that solving a POMDP directly is infeasible even for the simplest problems [31].

Advances have been made in applying approximate POMDP algorithms to robotic applications [11]. However the optimisation often requires a discretisation of the action space which is restrictive for tasks which are naturally continuous. In the case actions are considered continuous, a local optimisation with quantifiable actions (marcos) [36] or alternatively heuristic approaches [22], based on the most likely state, can be applied. These approaches concede global optimality for a faster approximate solutions which depending on the

problem is often close to optimality. Solving continuous actions POMDPs via reinforcement learning is difficult as the exploration-exploitation makes the dimensionality of the problem daunting which lead to the development of local approximate methods in belief space planning [cite].

In this paper we propose an approximate POMDP methods for continuous belief-state and action space. We introduce a Fitted Policy Iteration (FPI) Actor-Critic (AC) Reinforcement Learning (RL) method in which sample episodes are provided by human teachers in a Programming by Demonstration (PbD) framework. From the demonstrations provided by the teachers we hypothesis that a good mixture of explorative-exploitative behaviour is present. We have previously shown [9] that humans exhibit risk-prone and averse behaviour which would, as hypothesised, constitutes an ideal training set for RL, thus removing the need for a costly autonomous exploration. By applying a Fitted RL to the training set we learn a value function which we used to train a belief-space Gaussian Mixture Model policy.

We consider a plug power-socket search and connection task, also known as Peg-in-Hole (PiH), in which a robot apprentice must learn how to localise a power socket and then establish a connection. No vision system is used during the task and we solely rely on haptic information, provided via force-torque sensor mounted on the end-effector of the robot. We chose to not use vision for two reasons. The first is to validate that humans can be viable as expert teachers under these conditions which can be disorientating for humans. The second is that PiH is a very important component in manufacturing processes and

*Corresponding author

Email addresses: guillaume.dechambrier@epfl.ch (Guillaume de Chambrier), aude.billard@epfl.ch (Aude Billard)

we seek to demonstrate that we accomplish the task without the need of a vision system which would result in additional costs.

The rest of the paper is organised as follows: Section 2 overviews the literature of Peg-in-hole (PiH) and Actor-critic Fitted Reinforcement Learning. Section 3 details the PiH-search task, the formulation of the belief space, the data recorded and the number of human teachers taking part. Section 4 presents the Fitted Policy Iteration (FPI) algorithm. Section 5 details the control architecture. Section 6 experiments are conducted to evaluate the FPI in the PiH-search task. Section 7, discussion and conclusion.

2. Related work

There are two research domains which are closely related to our work. The first is Fitted Reinforcement learning (also known as Batch or Experience replay) and the second is Peg-in-hole.

2.1. Peg-in-hole

The Peg-in-Hole (PiH) task is one of the most widespread steps in industrial assembly and manipulations processes, with examples including the assembly of vehicular transmission components [12] and valves [10]. To be successful, the estimated position of the robot’s end-effector and workpiece must be precise. Typically, the clearance between peg and hole is very small leaving little room for error.

All approaches use to some extent a vision system [23] to estimate the position of the workpiece. Given the peg’s estimated position with respect to the hole an insertion strategy has to be carried since the hole will be occluded by the robot’s manipulator. One approach is to apply blind search patterns, such as circular motions [12], which do not consider actual state uncertainty. These approaches work well when the plug or peg is within the vicinity. In our work we consider no visual information which leads to high state uncertainty making the direct application of such blind search methods ill-suited.

Another approach consists of learning task space policies and gradually adapt its parameters based on a reference Force/Torque profile. In [38] the authors learned a time-dependent Dynamic Movement Primitive (DMP) [33] Cartesian end-effector policy for the Cranfield benchmark object from human teleoperated demonstrations. Similarly in [25, 1], a F/T profile is encoded separately by a regressor function along the DMP policy. Successive refinements of the DMP policy are achieved through using force feedback to adapt the parameters of an admittance controller such to reproduce the same F/T (encoded by a separate regressor).

Reproducing exactly the same force torque profile for the full trajectory which is encoded in a time dependent dynamical system might be unnecessary as the force torque profile is predominantly useful during the final stage of the PiH task, where the insertion can cause jamming. The force torque information can be used to rectify this problem [20, Chap. 5].

Reinforcement learning has also been applied to PiH. In [19] a DMP policy is initialised with kinesthetic demonstrations of picking up a pen. The recorded Cartesian trajectories are encoded in a parameterised DMP policy and augmented with a

F/T profile. After 110 trials the policy was found to be a 100% successful. In [17] a 18 dimensional input and a 6 dimensional output (linear and angular velocity) neural network is learned. After a 100 episodes the policy was shown to be successful. Our work is similar in its approach, however we will not be considering autonomous rollouts common in RL, but will rely solely on the data provided by human teachers.

2.2. Actor-Critic & Fitted Reinforcement Learning

Actor-critic [35, Chap. 6.6] have two separate parameterisation of the policy (actor) and value function (critic). It has been reported and proven [16] to be faster than policy search methods as the variance in the gradient estimate is smaller. The advantage of an AC is that the policy can be chosen such that it is computationally efficient in evaluating actions whilst the value function can have a more complex representation.

To guarantee convergence (in model based RL) during temporal difference learning, the value function approximators has to be an averager (tile coding, k-nearest-neighbour, locally weighted averaging) [15]. The extension to a model-free approach with a kernel function approximator (locally weighted averaging, the kernel is a Gaussian function) known as Kernel-Based Approximate Dynamic Programming (KBDP) [28] has proven to be globally optimal in a continuous-space framework. This leads to the wider application of Batch RL methods such as Fitted Value Iteration (FVI) [6] and Fitted Q-Iteration (FQI) [14] (Q-approximator is a random forest ensemble), [26] in RL problems. By remembering all the state transition pairs and by applying multiple synchronous Dynamic Programming (DP) and function approximation updates, the problem of diverging value function approximators is resolved.

Retaining all the data makes it in practice easy to apply function approximators which are not averagers, such as neural networks, to RL problems. A successful example was Neural Fitted Q-Iteration (NFQI) [32] which uses a multi-layer perceptron to represent the Q-function for the cart-pole and mountain car problems and shows rapid convergence to optimal policies. It has since been used in many extensions, [29], [2]. This has lead to the application of more sophisticated regression methods such Deep Learning, such as Deep Fitted Q-iteration (DFQ) [21] which is used to learn visual control policies and with recent work including learning to play ATRI and ping-pong games [24], [18].

The reader is referred to [7] and [37, Chap 2] for a literature review which includes a taxonomy of Batch RL methods and to for a concise description Batch RL beginning at its origins, how it became popular with Fitted RL approaches and its continuation into Deep Learning.

The Fitted Policy Iteration which we apply to our belief space PiH search task is part of this family of methods. We chose an on-policy approach to avoid the maximisation over the actions, as we are in continuous action space. We use a Gaussian Mixture Model to parameterise the policy and a Locally Weighted Regression (LWR) as the value function approximator.

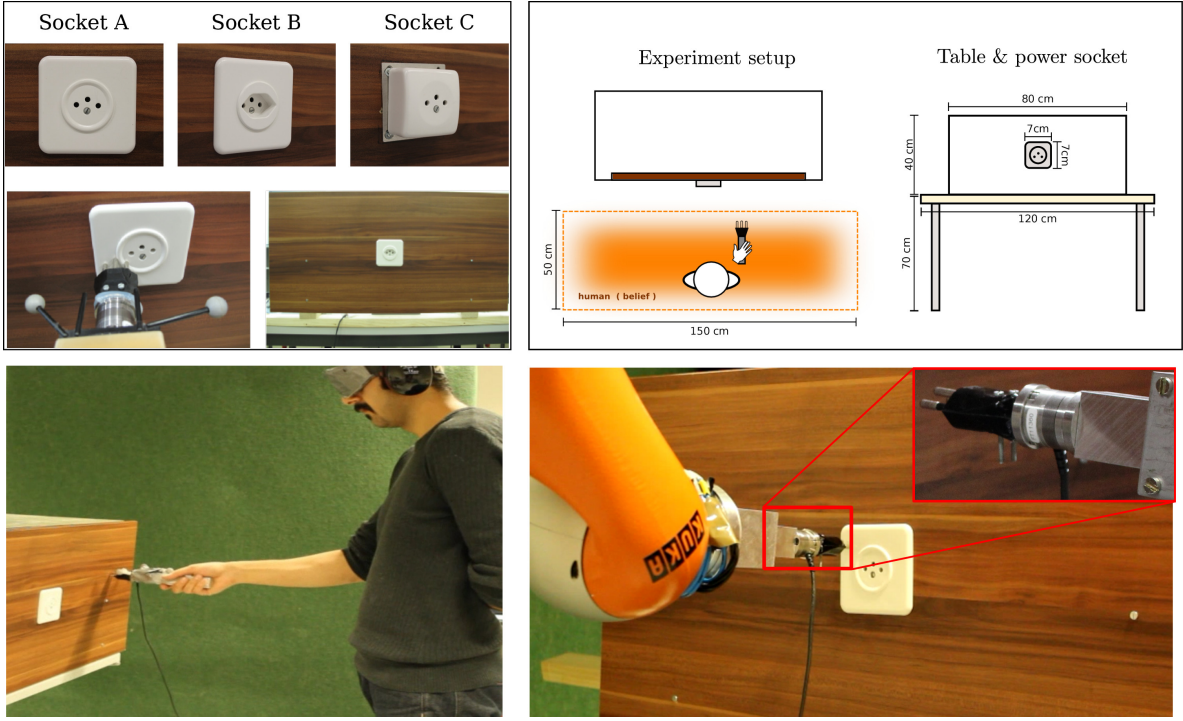


Figure 1: **Peg-in-Hole search task setup.** *Top-left:* Three different sockets are used, socket A will be only used to gather training data whilst socket B and C will be used evaluation purposes; *Bottom-left:* A participant (human teacher) is blindfolded and placed within the orange rectangular area always facing the wall. *Top-right:* Dimensions of the the wall and socket, and the orange area illustrates the possible starting locations. *Bottom-right:* The KUKA LWR robot is equipped with a peg holder mounted with an ATI force torque sensor, it is reproducing a search and connection policy learned from the human demonstrations.

3. Experiment methods

Figure 1 (*Top-right*), illustrates the PiH-search task. The orange area represents the teachers starting area and is assumed prior knowledge. The sockets are always positioned at the center of a fake wall (wooden plank) which is clamped to a table. We consider one type of plug, Type J¹, and three different power sockets. Power socket *A*, has a ring around its holes, *socket B* has a funnel, which we hypothesize should make it easier to connect, and *socket C* has a flat elevated surface. See Figure 1 (*Top-left*) for an illustration.

The human teacher holds the plug which is attached to a cylindrical handle with an ATI 6 axis force torque sensor (Nano25²) to provide **raw** wrench $\phi \in \mathbb{R}^6$ measurements. We define the **actual** measurement to be a function of the raw wrench, $\tilde{y}_t = h(\phi_t)$, which is a binary feature vector. The feature vector encodes whether a contact is present and the direction in which it occurs, which is discretized to the four cardinalities.

On top of the cylinder there is a set of markers used by a motion capture system OptiTrack³ (which has millimeter tracking accuracy) to measure both linear, $\dot{x} \in \mathbb{R}^3$, and angular velocity, $\omega \in \mathbb{R}^3$, at each time step which is recorded at a rate of 100 Hz along with the F/T information.

The human's location belief is represented by a probability density function (pdf) which is assumed to be uniformly dis-

tributed in the orange area and that all subsequent beliefs can be inferred from the measured velocity and measurements provided by the ATI and OptiTrack sensors.

3.1. Belief state

The belief probability density function, $p(x_t|y_{0:t}, \dot{x}_{1:t})$, is a Point Mass Filter (PMF) [4, p.87], which is a non-parametric Bayesian filter. In Figure 2 (*Left*) we illustrate different time segments of the location belief recording during a demonstration. In Figure 2 (*Right*) we illustrate the likelihood when an edge is sensed. A PMF is chosen to represent the believed location of the plug as the sensing likelihoods are non-gaussian and lead to multi-modal distributions.

The pdf is high dimensional and thus it is impractical to directly learn a statistical policy $\pi_\theta : p(x_t|y_{0:t}, \dot{x}_{1:t}) \rightarrow \dot{x}$ without some form of compression. We compress it to a belief space vector $b_t = [\hat{x}_t, U]^T$ composed of the maximum a posteriori, $\hat{x}_t \in \mathbb{R}^3$, and the differentiation entropy, $U = H\{p(x_t|y_{0:t}, \dot{x}_{0:t})\} \in \mathbb{R}$.

Each participant's demonstration results in a dataset $D = \{\dot{x}_{1:T}^{[i]}, \omega_{1:T}^{[i]}, \phi_{1:T}^{[i]}, b_{1:T}^{[i]}\}$, where the upper index $[i]$ references the i th search trajectory (also one execution of the task or one episode) and subscript $1 : T$ denotes the time steps during the trajectory from initialisation $t = 1$ until the end $t = T$.

3.2. Participants and experiment protocol

To perform the PiH search tasks we recruited 10 student volunteers to be teachers (all male Master's and PhD students).

¹<http://www.iec.ch/worldplugs/typeJ.htm>

²<http://www.ati-ia.com/products/ft/sensors.aspx>

³<http://www.optitrack.com/>

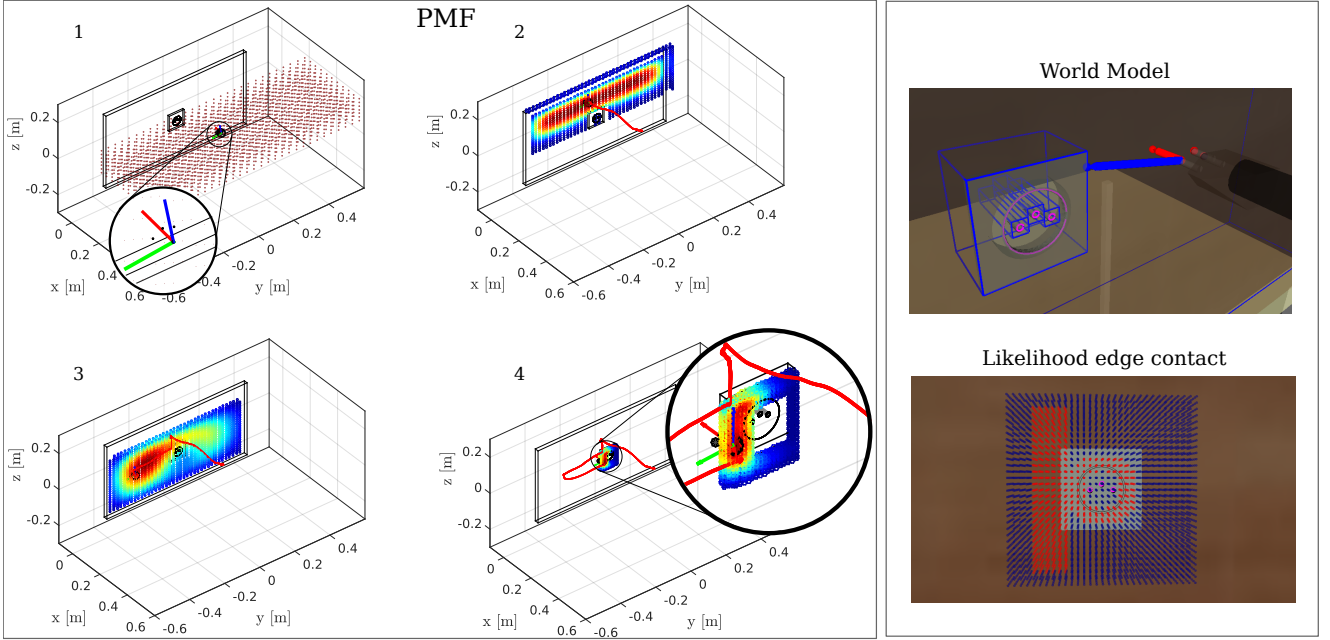


Figure 2: *Left:* Point Mass Filter (PMF) update of a particular human demonstration. (1) Initial uniform distribution spread over the starting region. Each grid cell represents a hypothetical position of the plug. The orientation is assumed to be known. (2) First contact, the distribution is spread across the surface of the wall. The red trace is the trajectory history. (3) motion noise increases the uncertainty. (4) The plug is in contact with a socket edge. *Right:* **World model**: The plug is modelled by its three plug tips and the wall and sockets are fitted with bounding boxes. **Likelihood**: The plug enters in contact with the left edge of the socket. As a result, the value of the likelihood in all the regions, x_t , close the left edge take a value of one (red points) whilst the others have a value zero (blue points) and areas around the socket's central ring have a value of one.

The participants were aged between 24 and 30 with an average age of 26 years and a standard deviation of 2.4 years. Each participant carried out 30 demonstrations of the PiH search-task and each session lasted approximately 50 minutes and never exceeded one hour. The 10 participants were divided equally in two groups, A and B. Each member of group A began by performing 15 PiH searches with socket A, followed by a 10 minute break, finishing with an additional 15 searches with socket B. The members of group B performed the same protocol starting with socket B and ending with socket A. Figure 3 summarises a walk through of the experiment. The only exclusion criteria was the inability of the subject to accomplish the task. All participants gave written consent for taking part in this study. A total of 300 demonstrations were gathered. Both groups A and B took 9 ± 10 s to find the socket's edge, regardless of the socket type. This is to be expected since the sockets are at the same location. It took a further 8 ± 7 s on average for group B to connect socket B and 12 ± 10 s on average for group A to connect socket A. As we can see this is not a straight forward task when considering the sensory deprivation. See Figure 4 (*Bottom*) for the time taken to connect the plug to the socket.

4. Learning Actor and Critic

We learn two policies. The first policy maps from belief space to linear velocity $\pi_{\theta_1} : b_t \mapsto \dot{x}_t$ and the second from sensed wrench to angular velocity, $\pi_{\theta_2} : \phi_t \mapsto \omega_t$. The belief policy π_{θ_1} is learned in a Fitted Actor-Critic framework and the wrench policy π_{θ_2} directly from the demonstrated data as was

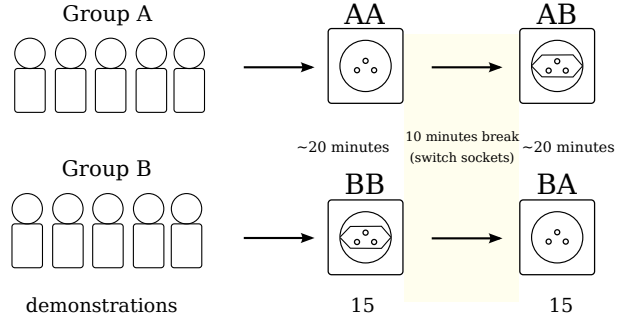


Figure 3: Experiment protocol. The participants are divided in two groups of 5, Group A begins with socket A and after a short break repeats the task with socket B. The same logic holds for Group B. For each socket 15 executions of the task are recorded.

done in [20, Chap. 5], which proved to be efficient in overcoming jamming during the final insertion step of PiH. Our objective is to maximise the parameters of the policy, $\pi_{\theta_1} : b \mapsto \dot{x}_t$, with respect to the value function:

$$V^{\pi_{\theta_1}}(b) = \mathbb{E}_{\pi_{\theta_1}} \left\{ \sum_{t=0}^{\infty} \gamma^t r_{t+1} | b_t = b, \pi_{\theta_1} \right\} \quad (1)$$

where $r_t \in \mathbb{R}$ is the reward and $\gamma \in [0, 1]$ the discount factor. It is the expected future reward given the current belief state and policy. For our PiH-search task we assign a reward of $r = 0$ at each time step until the goal (plug-socket connection) is achieved, where a reward of 100 is given, $r_T = 100$. Given the continuous nature and dimensionality of the belief space

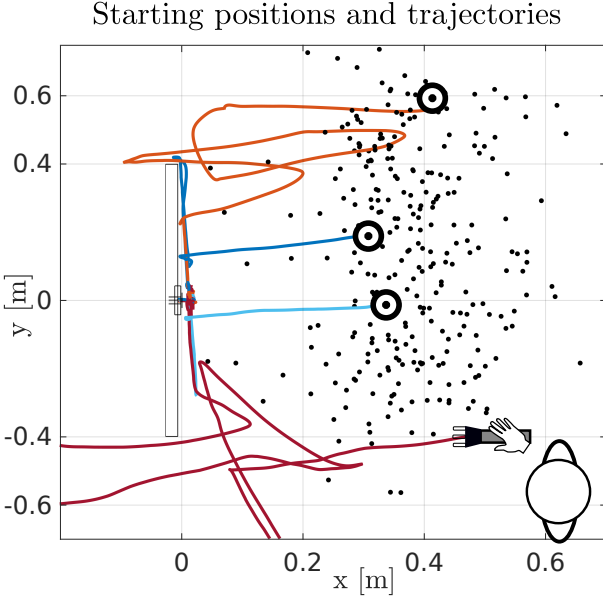


Figure 4: Top: Black points represent the starting position of the end-effector for all the demonstrations. Four trajectories are illustrated.

we use Locally Weighted Regression [3] (LWR) as a function approximator of the value function, $V^\pi(b)$.

In an Actor-Critic setting, the temporal difference error, $\delta_t^\pi = r_{t+1} + \gamma V^\pi(b_{t+1}) - V^\pi(b_t)$, of the value function is used as a learning signal to update simultaneously itself and the actor (the policy).

4.1. Actor & Critic

Both the linear and angular velocity policies are parameterised by a Gaussian Mixture Model (GMM), Equation 2.

$$\pi_{\theta_1}(\dot{x}, b) = \sum_{k=1}^K w^{[k]} g(\dot{x}, b; \mu^{[k]}, \Sigma^{[k]}) \quad (2)$$

The parameters $\theta = \{w^{[k]}, \mu^{[k]}, \Sigma^{[k]}\}_{1,\dots,K}$, are the weights, means and covariances of the individual Gaussian functions, $g(\cdot)$,

$$\mu^{[k]} = \begin{bmatrix} \mu_{\dot{x}}^{[k]} \\ \mu_b^{[k]} \end{bmatrix}, \Sigma^{[k]} = \begin{bmatrix} \Sigma_{\dot{x}\dot{x}}^{[k]} & \Sigma_{\dot{x}b}^{[k]} \\ \Sigma_{b\dot{x}}^{[k]} & \Sigma_{bb}^{[k]} \end{bmatrix}$$

where $\sum_k w^{[k]} = 1$, $\mu_{\dot{x}}^{[k]} \in \mathbb{R}^3$ and $\mu_b^{[k]} \in \mathbb{R}^4$. In both cases we use the Bayesian Information Criterion to determine the number of Gaussian functions. In the next section, we will show how the parameters of π_{θ_1} can be adapted by the value function.

4.2. Fitted Policy Iteration

Policy evaluation. To learn the value function we take Fitted RL [14] approach. This is an offline method which applies multiple sweeps of the Bellman backup operator over a dataset of tuples $\{(b_t^{[i]}, r_t^{[i]}, b_{t+1}^{[i]})\}_{i=1,\dots,M}$ until the Bellman residual, $\|\hat{V}_{k+1}^\pi(b) - \hat{V}_k^\pi(b)\|$, converges, see Algorithm 1.

Algorithm 1: Fitted Policy Evaluation

```

input :  $\epsilon, \{(b_t^{[i]}, r_t^{[i]}, b_{t+1}^{[i]})\}_{i=1,\dots,M}$ 
output:  $\hat{V}_k^\pi(b_t)$ 
1 while  $\|\hat{V}_{k+1}^\pi(b) - \hat{V}_k^\pi(b)\| < \epsilon$  do
2    $\hat{V}_{k+1}^\pi(b_t) = \text{Regress}(b, r_t + \gamma \hat{V}_k^\pi(b_{t+1}))$ 

```

Most Fitted RL methods have focus on learning the Q-value function directly (Fitted Q-Iteration) [27, 14, 32]. Although this solves the control problem it requires discretisation of the action space or assumes quantifiable actions, as the Q-Bellman backups such to easily achieve the maximisation $\max_{\dot{x}_{t+1}} \hat{Q}(\dot{x}_{t+1}, b_{t+1})$. Given the dimensionality and continuity of our problem we assume this to be unrealistic. As such we opt for an on-policy approach mentioned above.

Policy improvement. We update the Actor policy given the Critic value function through a modification of the Maximisation step in Expectation-Maximisation (EM) for Gaussian Mixture Models. We refer to this modification as Q-EM which is strongly related to a Monte-Carlo EM-based policy search approach [13, p.50].

The reward of a demonstrated trajectory (one episode) is given by the discounted return, Equation 3,

$$R(b^{[i]}, \dot{x}^{[i]}) = \sum_{t=0}^{T^{[i]}} \gamma^t r(b_t^{[i]}, \dot{x}_t^{[i]}) \quad (3)$$

where the index i stands for the i th episode. All policy gradient approaches seek to find a set of parameters, θ , of the Actor, which will maximise the expected reward, equivalent to maximising Equation 4,

$$\begin{aligned} J(\theta) &= \mathbb{E}_{p_\theta}\{R\} \\ &= \sum_{i=1}^N \underbrace{\left(\prod_{t=0}^{T^{[i]}} \pi_\theta(\dot{x}_t^{[i]}, b_t^{[i]}) \right)}_{p_\theta(\tau_i)} R(\tau_i) \end{aligned} \quad (4)$$

where $\tau_i = \{(\dot{x}_0, b_0), \dots, (\dot{x}_T^{[i]}, b_T^{[i]})\}$ are the state-action samples of the i th episode. To find the parameters which maximise the cost function, $\arg \max_\theta J(\theta)$, its derivative is set to zero. As this cannot be done directly, the logarithmic lower bound is of the cost function is maximised instead which results in Equation 5, see [13, p.50] for the derivation.

$$\nabla_\theta Q(\theta, \theta') = \sum_{i=1}^N \sum_{t=0}^{T^{[i]}} \nabla_\theta \log \pi_\theta(\dot{x}_t^{[i]}, b_t^{[i]}) Q^{\pi_{\theta'}}(\dot{x}_t^{[i]}, b_t^{[i]}) \quad (5)$$

In the above equation θ' are the parameters used to generate the trajectories during the E-step. In most policy search approaches the policy is conditioned on the state space, $\pi_\theta(\dot{x}_t | b_t)$. This would lead to a complex expressions in the maximisation of Equation 5 and is restrictive in the case of the GMM as it fixes the state space parameters $\mu_b^{[k]}, \Sigma_{bb}^{[k]}$ (and partially $\Sigma_{\dot{x}b}^{[k]}$). Instead

$$\boldsymbol{\mu}_{\text{new}}^{[k]} = \frac{\sum_{j=1}^M \gamma_k(\mathbf{x}^{[j]}) Q^{\pi_{\theta'}}(\mathbf{x}^{[j]}) \mathbf{x}^{[j]}}{\sum_{j=1}^M \gamma_k(\mathbf{x}^{[j]}) Q^{\pi_{\theta'}}(\mathbf{x}^{[j]})}$$

$$\Sigma_{\text{new}}^{[k]} = \frac{\sum_{j=1}^M \gamma_k(\mathbf{x}^{[j]}) Q^{\pi_{\theta'}}(\mathbf{x}^{[j]})(\mathbf{x}^{[j]} - \boldsymbol{\mu}^{[k]})(\mathbf{x}^{[j]} - \boldsymbol{\mu}^{[k]})^T}{\sum_{j=1}^M \gamma_k(\mathbf{x}^{[j]}) Q^{\pi_{\theta'}}(\mathbf{x}^{[j]})}$$

$$w_{\text{new}}^{[k]} = \frac{\sum_{j=1}^M Q^{\pi_{\theta'}}(\mathbf{x}^{[j]}) \gamma_k(\mathbf{x}^{[j]})}{\sum_{j=1}^M Q^{\pi_{\theta'}}(\mathbf{x}^{[j]})}$$

Figure 5: Q-EM Maximisation of the GMM parameters. We used the same notation and derivation as in [5, Chap. 9.2.2], where $\gamma_k(\mathbf{x}^{[j]})$ is the responsibility factor, denoting the probability that data point $\mathbf{x}^{[j]} = [\dot{x}^{[j]}, b^{[j]}]^T$ belongs to Gaussian function k .

we optimise Equation 5 whilst considering the joint distribution $\pi_{\theta}(\dot{x}_t, b_t)$ and not the conditional $\pi_{\theta}(\dot{x}_t | b_t)$. This has two beneficiary outcomes. The first is that the input dimension (the state space) are no longer fixed allowing the basis functions of the GMM to move and the second benefit is that the optimisation of GMM parameters is very similar to those of the traditional EM. Setting the derivative of Equation 5 to zero and solving for the parameters $\boldsymbol{\theta} = \{w, \boldsymbol{\mu}, \boldsymbol{\Sigma}\}$ leads to a Maximisation update step of EM which is weighted by $Q^{\pi_{\theta'}}$, see Figure 2.

As we learned the value function in the policy evaluation step, we use the advantage function

$$A^{\pi_{\theta}}(\dot{x}_t, b_t) = Q^{\pi_{\theta}}(\dot{x}_t, b_t) - V^{\pi_{\theta}}(b_t) = \delta_t^{\pi_{\theta}} \quad (6)$$

as a substitute for Q^{π} which we derive from the TD error. Assuming that our estimated value function, \hat{V}^{π} , is close to the true value function V^{π} , the TD error δ^{π} is an unbiased estimate of the advantage function. Using the advantage function as means of policy search is popular with methods such as Natural Actor Critic (NAC) [30].

2D example fitted policy iteration. To illustrate the mechanism of fitted policy iteration, we give a 2D example of its application, see Figure 6. The *Top-left* subfigure depicts 10 trajectories demonstrated by two teachers going from start (white circle) to goal (orange star) state. The optimal path is a straight line passing in between two obstacles. Neither teacher demonstrated the optimal straight path.

In the *Bottom-left*, a GMM is fitted $\pi_{\theta}(\dot{x}, x)$ to the teachers' data, using the standard EM-algorithm. Taking the policy to be the output of Gaussian Mixture Regression (GMR) $\mathbb{E}\{\pi_{\theta}(\dot{x}|x)\}$ we obtain different behaviours than those demonstrated by the

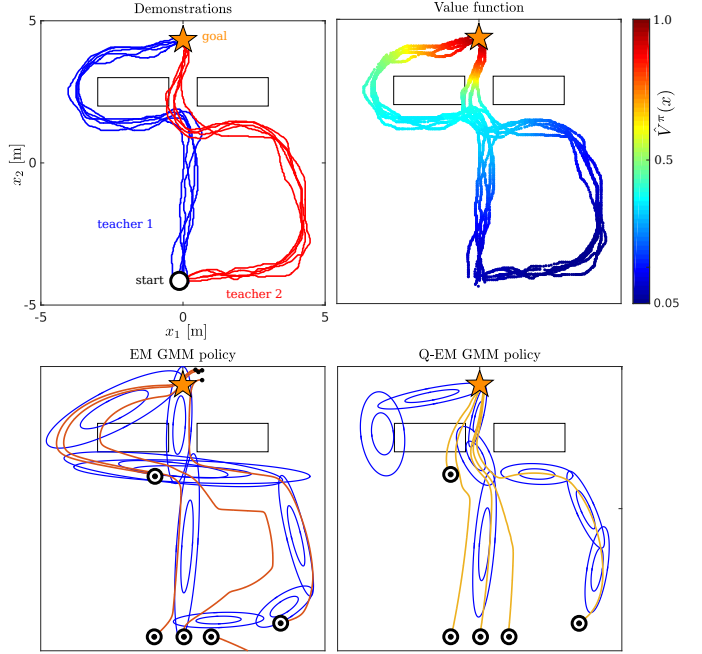


Figure 6: Fitted policy evaluation & improvement example. *Top-left*: The goal of the task is to reach the goal state. The first teacher (blue) demonstrates five trajectories which contours the obstacle in front of the goal. The second teacher (red) demonstrates 5 trajectories which initially deviate from the goal before passing between the two obstacles. *Bottom-left*: The EM algorithm is used to fit a GMM to the teachers' original data. The marginal $\pi_{\theta}(x)$ is plotted in blue and trajectories generated by the policy $\mathbb{E}\{\pi_{\theta}(\dot{x}|x)\}$ in orange. *Top-right Policy Evaluation*: Value function after fitted policy evaluation terminated, the reward function is binary, $r = 1$ at the goal and zero otherwise, and a discount factor $\gamma = 0.99$ is used. *Bottom-right Policy Improvement*: the GMM is learned with the Q-EM algorithm in which each data point's weight proportional to the advantage function.

human teachers. The GMR averages the different modes encoded by the Gaussian functions which results in a mixing of the original demonstrated behaviours. No trajectories of the GMR policy truly replicate the demonstrated behaviour.

In the *Top-right* subfigure, we apply fitted policy evaluation to the original demonstrated data (discount factor $\gamma = 0.99$ and reward $r = 1$ when the goal is reached and zero otherwise) and compute the value function.

The *Bottom-right* subfigure illustrates the GMM policy learned with the Q-EM algorithm. As the advantage function $A^{\pi}(x, \dot{x})$ is highest along the start-goal axis, data points following this gradient will have a higher weight. This results in a policy with better rollouts (closer to the optimal path) than the trajectories generated by the policy learned via standard EM.

Belief state fitted policy evaluation. FPI is applied to the data from demonstrations done on socket A. In Figure 7 we illustrate the value function of the most likely state. As expected, the value function is high closest to the socket and around the axis $z = 0$ and $y = 0$. When policy improvement via Q-EM is applied the Gaussian functions of the GMM will favour these locations.

In Figure 7 (*Middle-right*) we illustrate the best and worst trajectories in terms of the accumulated value function. We can

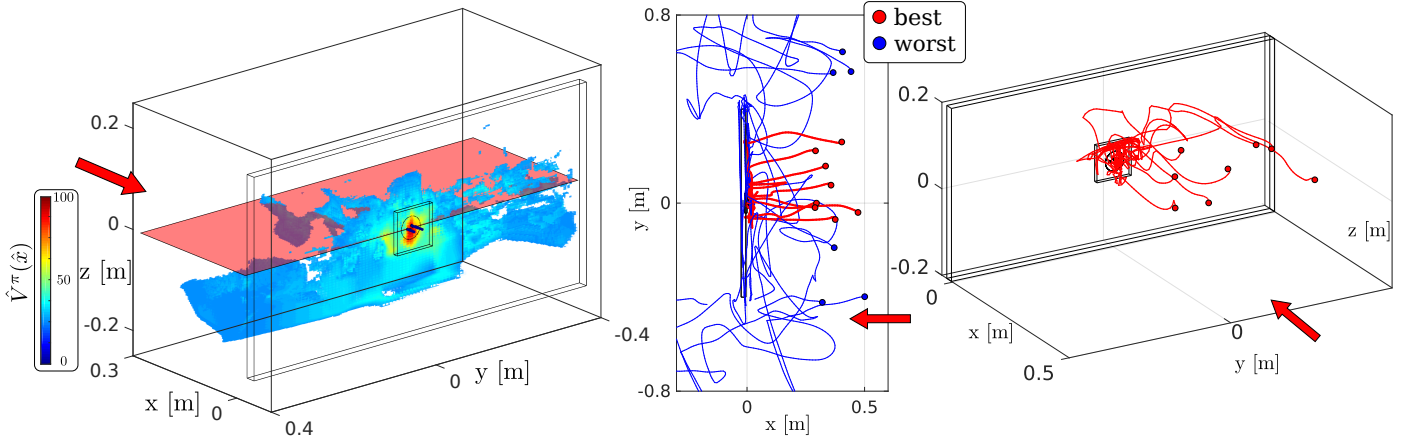


Figure 7: *Left:* LWR value function approximate $\hat{V}^\pi(\hat{x})$ for the most likely state \hat{x} . The red plane is to help visualise where the value function is above and below the axis $z = 0$. Only states with values above 0.25 are plotted. The red arrow indicates the heading of the human teacher when performing the search task. The discount factor was $\gamma = 0.99$ and the variance of the kernel variance of 1 [cm], which was set experimentally. *Middle-right:* Best and worst trajectories. The red demonstrated trajectories are the best in terms of the amount of value function gain whilst the blue are the worst. The red arrow indicates the teacher's heading. The blue trajectories tend towards the sides of the wall as the initial starting position is on the boarders of the wall. The red trajectories are centred along the y-axis of socket and tend to move in a straight line towards the wall whilst aligning themselves with the axis $z = 0$.

see that the five best trajectories (red) tend to be aligned with the socket (star position in front of socket), whilst the worst trajectories are towards the edges of the wall and tend to follow spiralling movements.

We learned two policies, one solely from the original human demonstrations which we call GMM and the second which is the result of **one iteration** of fitted policy iteration which we call Q-EM.

5. Control architecture

The direction to search is given by the conditional:

$$\pi_\theta(\dot{x}|b) = \sum_{k=1}^K w_{\dot{x}|b}^{[k]} g(\dot{x}; \mu_{\dot{x}|b}^{[k]}, \Sigma_{\dot{x}|b}^{[k]}) \quad (7)$$

which is a distribution over the possible normalised velocities. The function $g(\cdot)$ is a multivariate Gaussian function parameterised by mean $\mu_{\dot{x}|b}^{[k]} \in \mathbb{R}^{(3 \times 1)}$ and Covariance $\Sigma_{\dot{x}|b}^{[k]} \in \mathbb{R}^{(3 \times 3)}$. The subscript $\dot{x}|b$ indicates that the parameters are the result of the conditional. The reader is referred to [8], [34] for a detailed derivation of the conditional of a GMM. The learned model is multi-modal, as different search velocities are possible in the same belief state. Figure 8 illustrates the multi-modal vector fields of the conditional, Equation 7. In autonomous dynamical systems control, the velocity is obtained from the expectation of the conditional, Equation 7. However, the expectation which is a weighted linear combination of the modes, could result in unobserved behaviour or no movement if the velocities cancel out. As a result we use a modified version of the expectation operator which favours the current direction, Equation 8 - 9.

$$a(\dot{x}) = w_{\dot{x}|b}^{[k]} \cdot \exp(-\cos^{-1}(\langle \dot{x}, \mu_{\dot{x}|b}^{[k]} \rangle)) \quad (8)$$

$$\dot{x} = \mathbb{E}_a\{\pi_\theta(\dot{x}|b)\} = \sum_{k=1}^K \alpha_k(\dot{x}) \cdot \mu_{\dot{x}|b}^{[k]} \quad (9)$$

When the applied velocity mode is no longer present another direction is sampled. For example, when the robot enters in contact with a feature, greatly reducing the uncertainty, the current mode changes and a new search direction is computed. Figure 8 illustrates the policy vector field for GMM and Q-EM, both learned from teachers demonstrations.

5.1. Robot Implementation

The GMM policy $\dot{x} = \mathbb{E}_a\{\pi_\theta(\dot{x}|b)\}$ outputs a linear velocity which is normalised, $\dot{x} \in \mathbb{R}^{(3 \times 1)}$. The amplitude of the velocity is computed separately and modulated according to sensed forces on the end-effector. This search task is haptic and the end-effector of the robot is always in contact with the environment. To make the robot compliant with the environment we use an impedance controller in combination with a hybrid position-force controller. A hybrid controller targets a sensed force F_x , in the x -axis, of 3N. The y and z velocity components of the direction vector are given by Equation 9. This is insufficient for the robot to reliably surmount the edges of the socket, hence the vector field of the GMM is modulated in y and z -axis, Equation 10.

$$\dot{x} = R_y(c(F_z) \cdot \pi/2) \cdot R_z(c(F_y) \cdot \pi/2) \cdot \dot{x} \quad (10)$$

where R_y and R_z are (3×3) rotation matrices around the y and z -axis, and $c(F) \in [-1, 1]$ is a truncated scaling function of the sensed force. When a force F_z of 5N is sensed, a rotation of $R_y(\pi/2)$ is applied to the original direction resulting in the robot getting over the edge. The direction velocity is always

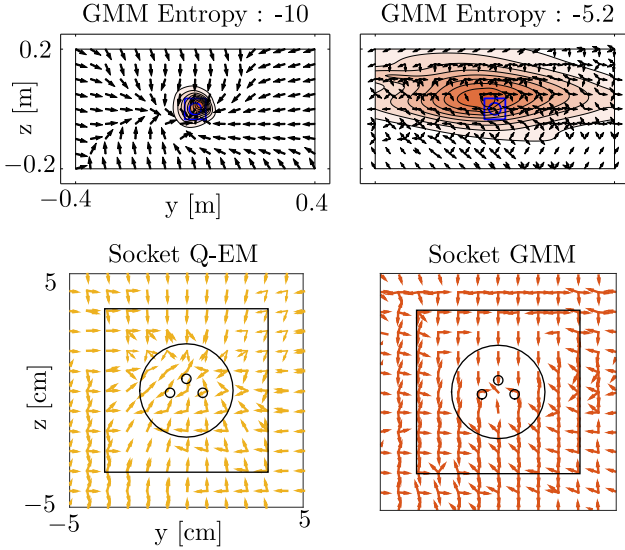


Figure 8: Q-EM and GMM policy vector fields. *Top*: The GMM policy is conditioned on an entropy of -10 and -5.2 . For the lowest entropy level, most of the probability mass is close to the socket area since this level corresponds to very little uncertainty; we are already localised. We can see that the policy converges to the socket area regardless of the location of the believed state. For an entropy of -5.2 we can see that the likelihood of the policy is present across wall. The vector field directs the end-effector to go towards the left or right edge of the wall. *Bottom*: The entropy is marginalised out, the yellow vector field is of the Q-EM and orange of the GMM. The Q-EM vector field tends to be closer to a sink and there is less variation.

normalised up to this point. The amplitude of the velocity is a proportional controller based on the believed distance to the goal. Figure 9 illustrates the complete control flow.

6. Results

We evaluate the following three aspects:

- 1. Distance taken to accomplish the goal** (connect plug to socket). We compare the Q-EM policy with a GMM policy learned through standard EM and a myopic Greedy policy. This highlights the difference between complicated and simplistic search algorithms and gives an appreciation of the problem's difficulty.
- 2. Importance of data** provided by human teachers. We evaluate whether it is possible to learn an improved GMM policy from Greedy demonstrations. This policy which we call Q-Greedy is used to test whether indeed human demonstrations are necessary. We evaluate whether it is possible to obtain a good policy from the two worst teachers' demonstrations as not all teachers are necessarily proficient at the task in question.
- 3. Generalisation.** We learn a policy to insert a plug into socket A which is located at the center of a wooden wall. We test the generalisation of the policy in finding a new socket location and whether the policy can generalise to sockets B and C, which were not used during the training phase.

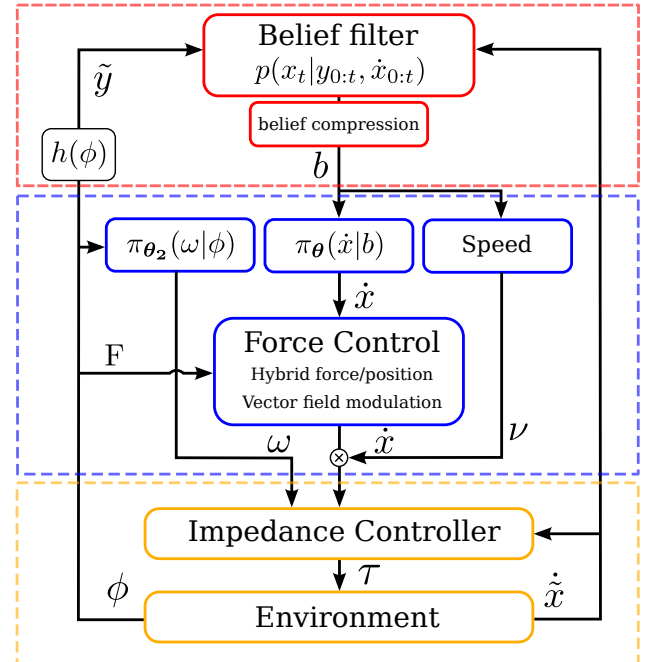


Figure 9: Control architecture. The PMF (belief) receives a measured velocity, \dot{x} , and a sensor measurement \tilde{y} and is updated via Bayes rule. The belief is compressed and used by both the GMM policy and the proportional speed controller.

We evaluate aspects 1) and 2) purely in simulation as finding the socket requires much less precision than establishing a connection and the physics of the interaction is simple. Aspect 3), the generalisation, is evaluated both in simulation, up to the point of localising the socket's edge, and on the KUKA LWR robotic platform for the connection phase of the task. The main reason for employing the robot is that the connection phase dynamics is complex and a simulation would be unrealistic. For the robot evaluation we consider the search starting already within the vicinity of the socket.

6.1. Distance taken to reach the socket's edge

We consider two search experiments which we refer to as **Experiment 1** and **2**, in order to evaluate the performance in terms of the distance travelled to reach the socket for the three search policies: GMM, Q-EM and Greedy. In these two experiments the task is considered accomplished when a search policy finds the socket's edge.

Experiment 1, three starting locations are chosen: *Center*, *Left* and *Right*. See Figure 10 (*Experiment 1 Top-left*), for an illustration of the initial condition. This setup tests the effect of the starting positions. A total of 25 searches are carried out for each of the search policies. The trajectory results show a clear difference between the trajectories generated by the GMM and Q-EM policies (*Experiment 1 Bottom-left*). The orange GMM policy trajectories go straight towards the wall, whilst the yellow Q-EM policy trajectories drop in height making them closer to the socket. *Experiment 1 Bottom-right*, we illustrate the distribution of the first contact with the wall for the *Center* initial conditions. The distribution of the first contact of the Greedy

method is uniform across the entire y -axis of the wall. It does not take into account the variance of the uncertainty. In contrast, the GMM policy remains centred with respect to the starting position and the Q-EM is even closer to the socket and there is much less variance in the location of the first contact.

Experiment 1 Top-right, we illustrate the quantitative results of the distance taken to reach the socket for all three experiments. For the *Center* initial condition, the Q-EM policy travels far less than the other search policies. Considering that the initial position of the search is 0.45 [m] away from the wall, the Q-EM policy finds the socket very quickly once contact has been established with the wall. For the *Right* and *Left* starting conditions both the GMM and Q-EM policies travel less distance to reach the socket, with a smaller variance when compared with the Greedy search policy.

Experiment 2, Figure 10 (*Experiment 2*), the initial true starting positions of the end-effector are taken from a regular grid, within the red cube (see *Experiment 1*), covering the whole start region, also used as the initial distribution for the human demonstrations. A total of 150 searches are carried out for each of the three policies. This experiment compares the search policies with the human teachers' demonstrations. The Human and GMM show similar distributions of searched locations. They cover the upper region of the wall and top corners, to some extent. These distributions are not identical for two reasons. The first is that the learning of the GMM is a local optimisation which is dependent on initialisation and number of parameters. The second reason is that the synthesis of trajectories from the GMM is a stochastic process.

For the Q-EM policy, the distribution of the searched locations is centred around the origin of the z -axis. The uncertainty is predominantly located in the x and y -axis. The Q-EM policy takes this uncertainty into consideration by restraining the search to the y -axis regardless of the starting position. The uncertainty is reduced when it is in the vicinity of the socket. The Greedy's policy search distribution is multi-modal and centred around the z -axis where the modes are above and below the socket. This shows that the Greedy policy acts according to the most likely state which changes from left to right of the socket, because of motion noise, resulting in left-right movements and little displacement. As a result the Greedy policy spends more time at these modes.

Experiment 2 Right, it is clear that all three search policies travel less to find the socket's edge compared with the teachers' demonstrations. All search policies are better than the human teachers with the exception of group BA, which is performing the task with socket A. The Q-EM policy remains the best.

We have shown that under three different experimental settings the Q-EM algorithm is predominantly the best in terms of distance taken to localise the socket. The GMM policy learned solely from the data provided by the human teachers also performs well in comparison to the human teachers and Greedy policy. We made, however a critical assumption in order to be able to use our statistical policy approach. This **assumption** is that a human teacher is proficient in accomplishing the task. If a teacher is not able to accomplish the task in a repetitive and consistent way so that a search pattern can be encoded by the

GMM, the learned policy will perform poorly. Next we evaluate the validity of this assumption and the importance of the training data provided by the human teachers.

6.2. Importance of data

We perform two tests to evaluate the importance of the teachers training data, which we will refer to as **Experiment 3**. Firstly we take the worst two teachers in terms of distance taken to find the socket's edge and learn a GMM and Q-EM policy separately from their demonstrations. In this way we can evaluate whether it is possible to learn a successful policy given a few bad demonstrations (15 training trajectories for each policy). Our second evaluation consists of using a noisy explorative Greedy policy as a teacher to gather demonstrations which can then be used to learn a new policy, which we call Q-Greedy.

Figure 11 (*Top-left*) illustrates 6 trajectories of teacher # 5. Once localised, the teacher would reposition himself in front of the socket and try to achieve an insertion. This behaviour was not expected since by losing contact with the wall, the human teacher no longer had sensory feedback necessary to maintain an accurate position estimate.

Figure 11 (*Bottom-left*) illustrates the value function of the belief state learned from the data of teacher # 5. The states with the highest values seem to create a path going from the socket towards the right edge of the wall. We proceed as before to learn a GMM policy from the raw data and a Q-EM policy in which the data points are weighted by the gradient of the value function. *Experiment 3 Middle-column*, we illustrate the resulting Marginalised Gaussian Mixture parameters for both the GMM and Q-EM policies and we plot 25 rollouts of each policy starting at the *Center* initial condition used in Experiment 1. We note that the trajectories of the GMM policy have much variance in contrast to the Q-EM policy, resulting from an excess of variance in the 15 original demonstrations given by the teacher. Too much variance is not necessarily good, a random (uniform) policy in terms of generated trajectories will have the most variance and is as expected extremely inefficient in achieving a goal. Furthermore there is insufficient data to encode a pattern for the GMM model. In contrast, the Q-EM finds a pattern by combining multiple parts of the available data and as a result fewer data points are necessary to achieve a good policy. This effect is clear in Figure 12, showing the performance of the GMM and Q-EM algorithms under the same initial conditions as in Experiment 1. For all the conditions and for both teachers #5 and #7 the Q-EM policy always does better than the GMM.

We also tested whether we could use the Greedy policy as a means of gathering demonstrations in order to learn a value function and train a Q-Greedy policy. We used the Q-Greedy algorithm in combination with random perturbations applied to the Greedy velocity, to act as a simple exploration technique. We performed a maximum of 150 searches, which terminated once the socket was found and used these demonstrations to learn a value function and GMM policy which we refer to as Q-Greedy. Figure 10 *Experiment 1-2 (bar plot)*, illustrates the statistical results of the Q-Greedy policy for Experiment 1 and

Experiment 1

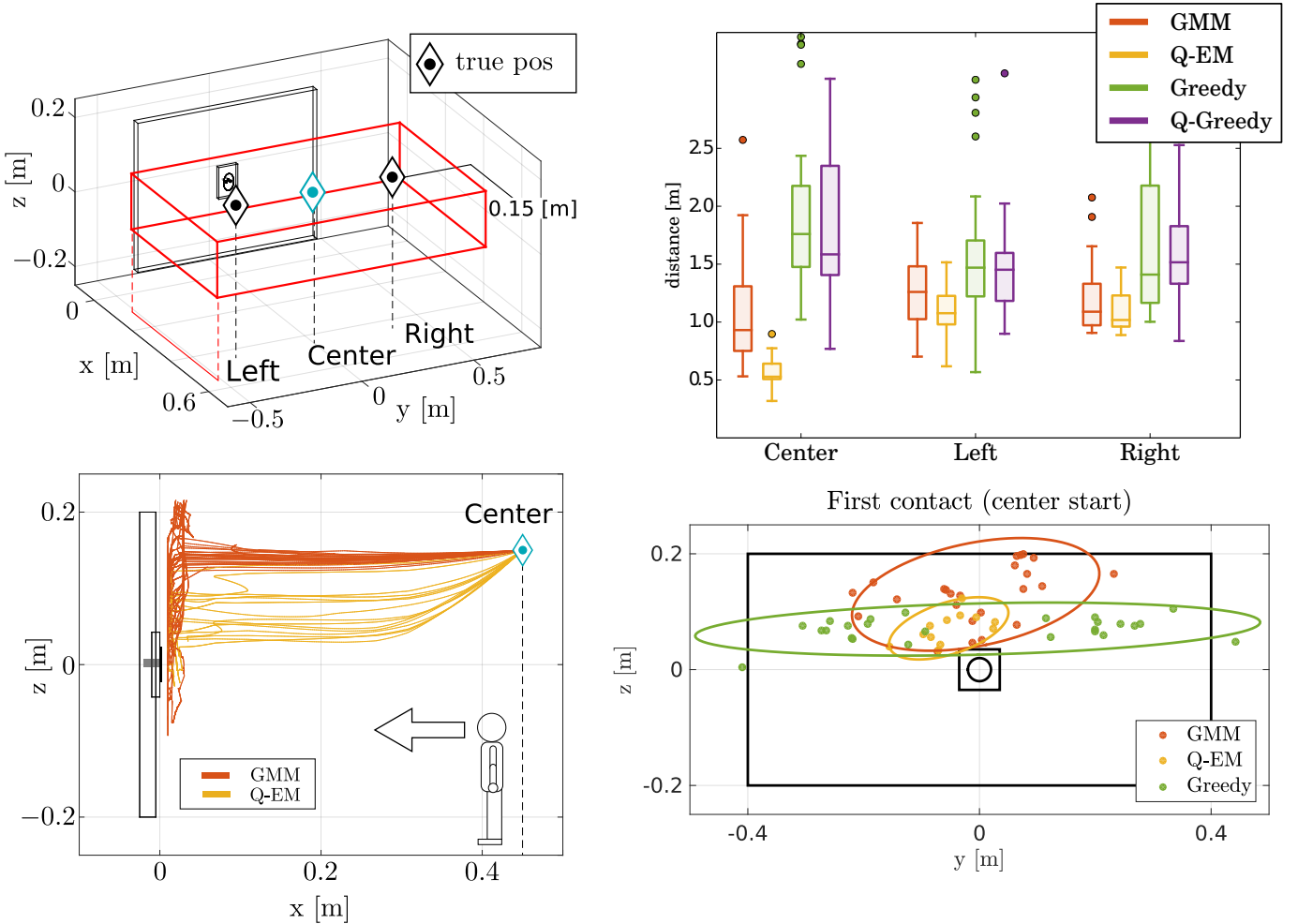


Figure 10: Two simulated search experiments. **Experiment 1:** *Top-left:* Three start positions are considered: *Left*, *Center* and *Right* in which the triangles depict true position of the end-effector. The red cube illustrates the extent of the uncertainty. *Bottom-left:* Trajectories of both the GMM (orange) and Q-EM (yellow) policies. For each start condition a total of 25 searches were performed for each search policy. *Bottom-right:* Distribution of first contact point giving the center initial starting condition. *Top-right:* Distribution of visited regions during the search for the socket's edge. The Q-EM policy's distribution is more centred along the axis $z = 0$. **Experiment 2:** *Left:* Distribution of the visited regions during the search for the socket's edge. The Q-EM policy's distribution is better than the humans with the exception of group BA. *Right:* Time taken to find the socket, the search algorithms are better than the humans with the exception of group BA.

Experiment 3

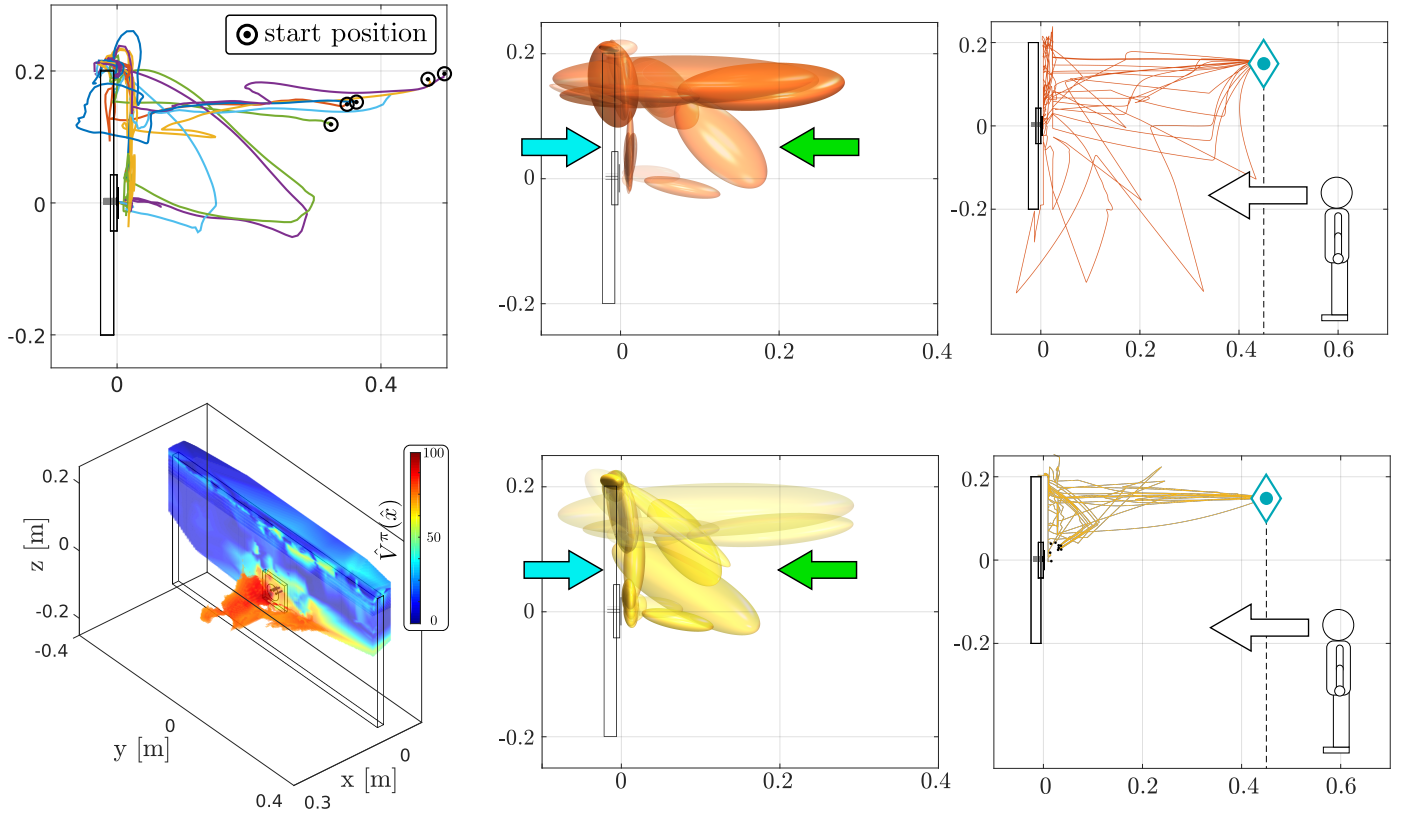


Figure 11: **Experiment 3** *Top-left:* Demonstrations of teacher #5. *Bottom-left:* Value function learned from the 15 demonstrations of teacher #5. The value of the most likely state is plotted. *Middle-column:* Most likely state parameters of the GMM and Q-EM learned from the demonstrations of teacher #5. *Right-column:* Rollouts of the policies learned from teacher #5. We can see that trajectories from the GMM policy have not really encoded a specific search pattern, whilst the Q-EM policy gives many more consistent trajectories which replicate to some extent the pattern of making a jump (no contact with the wall) from the top right corner to the socket's edge.

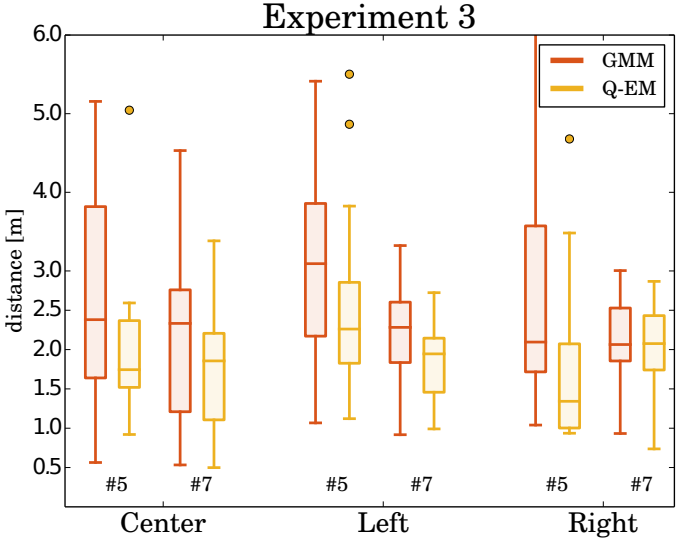


Figure 12: Results of a GMM and Q-EM policy under the same test conditions as Experiment 1. The Q-EM policy nearly always does much better than the GMM policy.

2 (purple bar chart), showing that there is no difference between two policies. Our exploration method is probably too simplistic to discover meaningful search patterns and we could probably devise better search strategies which would result in a good policy. However we have shown that human behaviour does already have a usable trade-off between exploration and exploitation which can be used to learn a new policy through our Fitted Policy Iteration framework.

6.3. Generalisation

So far we have trained and evaluated our policy within the same environment. To test whether our GMM policies can generalise to a new setting we changed the location of the socket to the upper right corner of the wall. The GMM was trained in the frame of reference of the socket and when we translated the socket's location it also translated the policy.

We use the same initial conditions of Experiment 1 with an additional new configuration named *Fixed*, in which both the true and believed location are fixed, blue triangle and circle. Figure 13 (*Left*) illustrates the trajectories of the three search policies for the *Fixed* initial condition. The Greedy policy moves in a straight line towards the top right corner of the table. As the true position is to the right, it takes the Greedy policy longer to find the wall in contrast to both the GMM and Q-EM policies. From the statistical results shown in Figure 13 (*Right*) we can see that for the *Fixed* and *Right* initial condition, which are similar, both GMM and Q-EM are better. However, for the *Center* and *Left* initial condition this is no longer the case. The Greedy method is better under this condition since the socket is close to informative features (it is located close to the edges of the wall). Once the end-effector has entered in contact with the wall the actions of the Greedy policy always result in a decrease of uncertainty, which was not the case when the socket was located in the center of wall. Thus in both the *Fixed* and

Right initial condition the Greedy method does worse because it takes longer to find the wall.

The GMM based policies are still able to generalise under different socket locations. In general, as the socket's location is moved further from the original frame of reference in which it was learned, the higher is the likelihood that the search quality degrades. We chose the upper right corner since it is the furthest point from the origin and the GMM and Q-EM policies were still able to find the socket. We note that the policy will always be able to find the socket once it has localised itself. This can be seen from the vector field of the GMM policy when the uncertainty is low, see Figure 8 on page 8. In this case the policy is a sink function with a single point attractor.

6.4. Distance taken to connect the plug to the socket

In this section we evaluate the distance taken for the policies and humans to establish a connection, after the socket has been found. We start measuring the distance from the point that the plug enters in contact with the socket's edge until the plug is connected to the socket. All the following evaluations are done on a KUKA LWR4 robot. The robot's end-effector is equipped with a plug holder on which is attached a force-torque sensor, the same holders used during the demonstration of the human teachers. In this way both the teacher and robot apprentice share the same sensory interface.

We chose to have the robot's end-effector located to the right of the socket and a belief spread uniformly along the z-axis. See Figure 14 for an illustration of the initial starting condition. This initial configuration was used to evaluate the search policies for the three different sockets, see Figure 1 on page 3 for an illustration of the sockets. The same initial configuration for the evaluation of the three sockets was kept in order to observe the generalisation properties of the policies. As a reminder we used only the training data from demonstrations acquired during the search with socket A. Socket B has a funnel which should make it easier to connect whilst socket C should be more difficult as it has no informative features on its surface.

For each of the sockets we performed 25 searches starting from the same initial condition. In Figure 14 (*Left*) we plot the trajectories of each of the search methods for socket A. The GMM reproduces some of the behaviour exhibited by humans, such as first localising itself at the top of the socket before trying to attempt to make a connection. The Q-EM algorithm exhibits less variation than the GMM and tends to pass via the bottom of the socket to establish a connection. The Greedy method in contrast is much more stochastic since it does not take into consideration the variance of the uncertainty but tries instead to directly establish a connection. In Figure 14 (*Right*) illustrates a typical rollout of the GMM search policy for both socket A and C. Once a contact is made with the socket's edge the policy tends to stay close to informative features and tends to wander vertically up and down. Only when the uncertainty has been reduced does the GMM policy try to go towards the socket's connector.

The GMM and Q-EM policies are able to generalise to both socket B and C, as the geometric shape and connector interface

Experiment 4

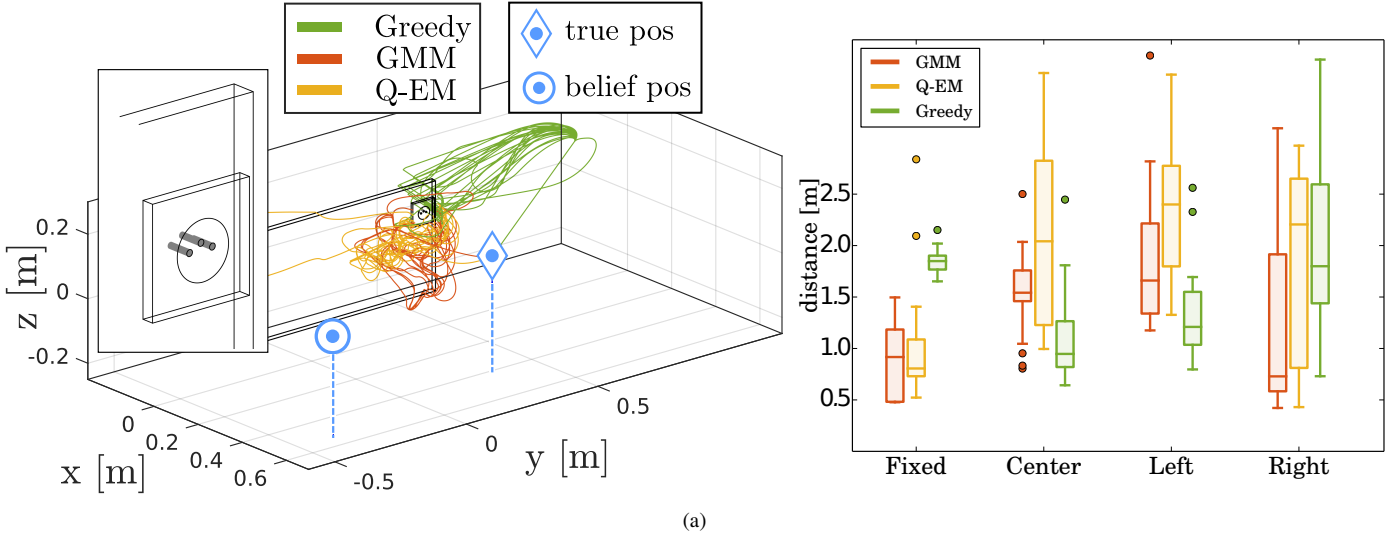


Figure 13: **Experiment 4** Evaluation of generalisation. The socket is located at the top right corner of the wall. We consider a *Fixed* starting location for both the true and believed location of the end-effector. The red square depicts the extent of the initial uncertainty, which is uniform. (b) Distance taken to reach the socket's edge. For the Fixed setup (see (a) for the initial condition), both the Q-EM and GMM significantly outperform the Greedy. The other three conditions are the same as for Experiment 1.

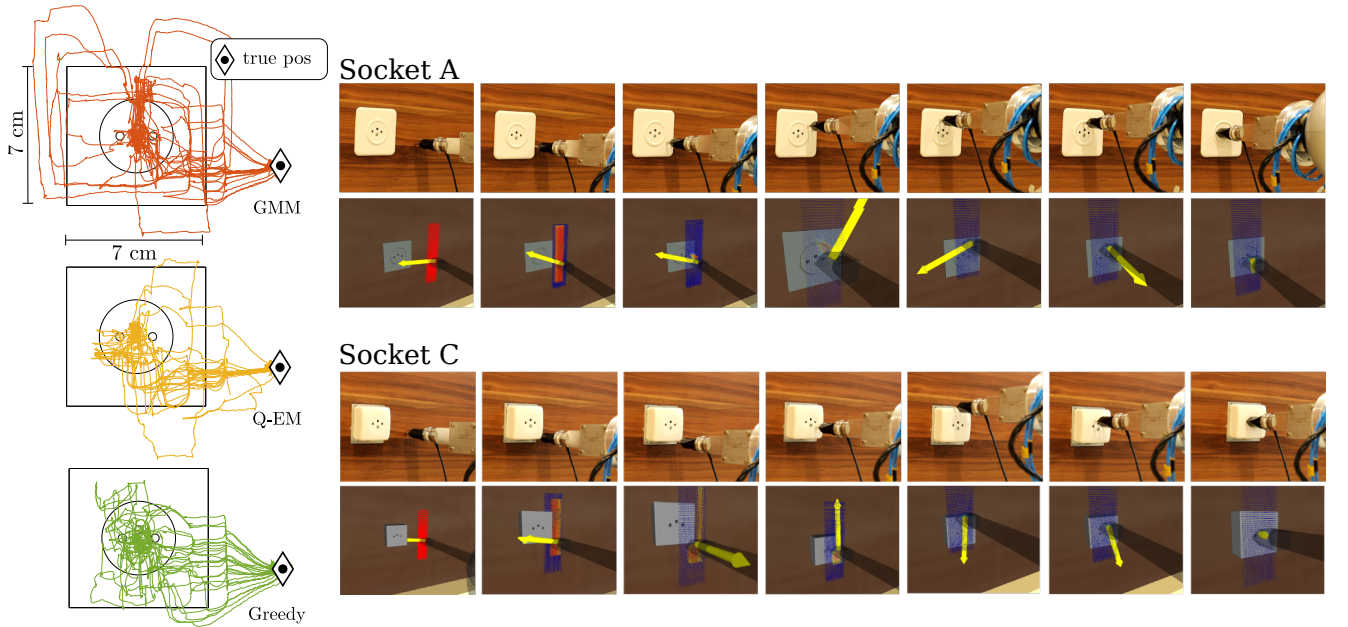


Figure 14: *Left:* 25 search trajectories for each of the three search policies for socket A. *Right:* KUKA LWR4 equipped with a holder mounted with a ATI 6-axis force-torque sensor. (a) The robot's end-effector starts to the right of socket A. The second row shows screen captures taken of ROS Rviz data visualiser in which we see the Point Mass Filter (red particles) and a yellow arrow indicating the direction given by the policy. In this particular run, the plug remained in contact with the ring of the socket until the top was reached before making a connection. *Bottom:* Socket C, same initial condition. The policy leads the plug down to the bottom corner of the socket before going the center of the top edge, localising itself, and then making a connection.

of the two sockets are similar to socket A. The local force modulation of the policy’s vector field, which is not learned, allows the end-effector to surmount edges and obstacles whilst trying to maintain a constant contact force in the x-axis. This modulation makes it possible for the plug to get on top of socket C.

Figure 15 (a) illustrates the statistics of the distance taken to establish a connection for all three sockets. For socket A both the Greedy and Q-EM are better than the GMM and the Q-EM has less variance in comparison to the Greedy searches. All three search methods are vastly superior, when compared to the human’s performance see Figure 15 (b-c).

The interesting point is that both the GMM and Q-EM algorithms perform better than the Greedy approach for socket C. Socket C has no informative features on its surface and as a result myopic policies such as the Greedy policy will perform poorly. However for socket A and B, the Greedy policy performs better as both of these sockets have edges around their connector point allowing for easy localisation. It can also be seen that most search methods perform better on socket B than A, since the funnel shape connector helps in maintaining the plug within the vicinity of the socket’s holes.

The discrepancy between the humans performance and the search policies can be attributed to many causes. One plausible reason is that the PMF probability density representation of the belief is more accurate than the human teachers position belief. Also, the motion noise parameter was fixed to be proportional to the velocity and the robot moves at gentle pace ($\sim 1 \text{ cm/s}$) as opposed to some of the human teachers. In actuality, humans are far less precise than the KUKA which has sub-millimetre accuracy.

7. Discussion & Conclusion

In this work we learned search policies from demonstrations provided by human teachers for a task which consisted of first localising a power socket (either socket A, B or C) and then connecting it with a plug. Only haptic information was available as the teachers were blindfolded. We made the assumption that the position belief of the human teachers was initially uniformly distributed in a fixed rectangular region of which they were informed and is considered prior knowledge. All subsequent beliefs were then updated in a Bayesian recursion using the measured velocity obtained from a vision tracking system, and wrench acquired from a force torque sensor attached to the plug. The filtered probability density function, represented by a Point Mass Filter, was then compressed to the most likely state and entropy.

Two Gaussian Mixture Model policies were learned from the data recorded during the human teachers’ demonstrations. The first policy, called Q-EM, was learned in an Actor-Critic RL framework in which a value function was learned over the belief space. This was then used to weight training datapoints in the M-step update of Expectation-Maximisation (EM). The second policy, called GMM, was learned using the standard EM algorithm, and considered all training data points equally, following in the footsteps of our initial approach [9]. Both the

Q-EM and GMM policies were trained with data solely from the demonstrations of the search with socket A.

We evaluated 4 different aspects of the learned policies. Firstly, we evaluated which of three policies, Q-EM, GMM and a Greedy policy, took the least distance to find the socket. We concluded that across three different Experiments the Q-EM algorithm always performed the best. It was clear that the Q-EM policy was less random and more consistent than the GMM policy as it tried to enter in contact with the wall at the same height as the socket thus increasing the chances of finding the socket.

Secondly, we tested the importance of the data provided by the human teachers. We took the worst two teachers and trained an individual GMM and Q-EM policy for each of them. We found that the performance of the Q-EM was better than the GMM in terms of distance travelled to find the socket. When qualitatively evaluating the trajectories of the GMM with respect to the Q-EM for the worst teacher, it is clear that the Q-EM policy managed to extract a search pattern, which was not the case for the GMM policy. We also tried to learn a Q-EM policy from the data provided by a Greedy policy with explorative noise and we found no improvement. From these results we conclude that the exploration and exploitation aspects of the trajectories provided by the human teachers is necessary.

Thirdly, we tested whether the two policies (GMM and Q-EM) were able to generalise to a different socket location. Under a specific condition, which we called *Fixed*, both policies were significantly better than the Greedy policy. However for the *Center* and *Left* initial conditions the Greedy policy performed better. For the initial conditions in which the Greedy policy enters in contact with the wall at an early stage, it also performs better than the GMM and Q-EM. The reason for this is that the actions taken by the Greedy policy in this setting will always result in a decrease of entropy when the location of the socket is close to a corner, as opposed to being in the center of the wall.

Fourthly, we evaluated all three policies on the KUKA LWR4 robot and found that all the policies did better than the human teachers. For socket A, on which both the GMM and Q-EM policies were trained, there is no clear distinction between the Q-EM and Greedy policy. On socket B, which was novel, the Greedy policy performed better than the statistical controllers, which we hypothesize was a result of a funnel which would make it easier for a myopic policy. For socket C, both the GMM and Q-EM policies performed better than the Greedy, as socket C has no features on its surface, this being a disadvantage for a myopic policy.

We conclude by making the observation that by simply adding a binary reward function in combination with data provided by human demonstrations, with Fitted reinforcement learning, we can learn a better policy without the need to perform expensive exploration-exploitation rollouts traditionally associated with reinforcement learning and designing complicated reward functions. This is especially advantageous when only a few demonstrations are available.

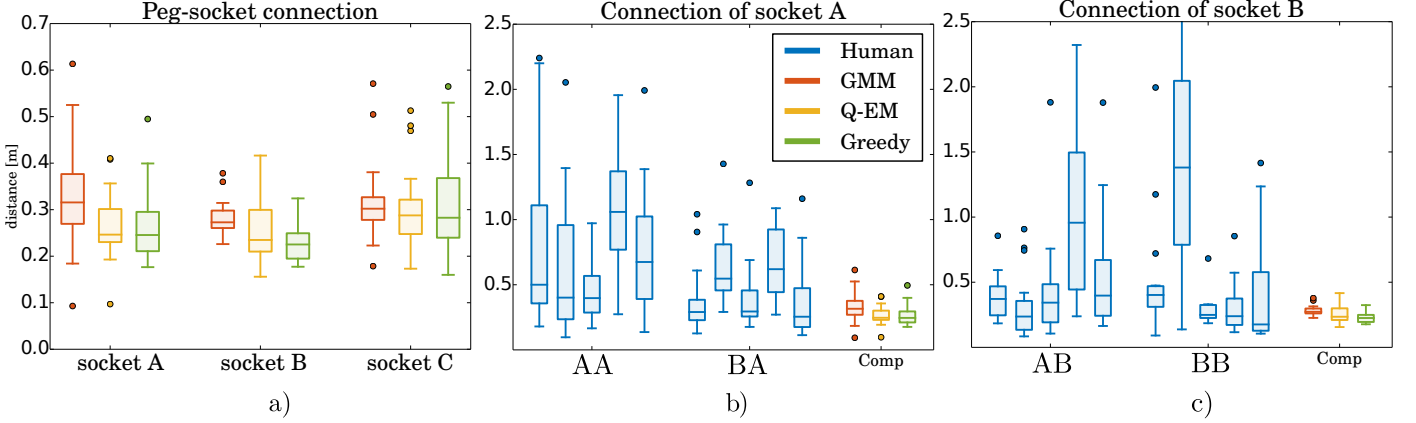


Figure 15: Distance taken to connect plug to socket once the socket is localised. (b) The human Group A are the set of teachers who first started with socket A. They had no previous training on another socket beforehand. Group BA first gave demonstrations on Socket B before giving demonstrations on Socket A. Group BA is better than Group AA at doing the task. This is most likely a training effect. However all policy search methods are far better at connecting the plug to the socket. (c) Both Groups AB and BB are similar in terms of the distance they took to insert the plug into the socket and as was the case for (b), the search policies travel less to accomplish the task.

- [1] Abu-Dakka, F., Nemec, B., Kramberger, A., Buch, A. G., Krüger, N., Ude, A., 2014. Solving peg-in-hole tasks by human demonstration and exception strategies. *Industrial Robot* 41 (6), 575–584.
- [2] Agostini, A., Celaya, E., July 2010. Reinforcement learning with a gaussian mixture model. In: *International Joint Conference on Neural Networks (IJCNN)*. pp. 1–8.
- [3] Atkeson, C. G., Moore, A. W., Schaal, S., 1997. Locally weighted learning. *Artificial Intelligence review*, 11–73.
- [4] Bergman, N., Bergman, C. N., 1999. Recursive bayesian estimation: Navigation and tracking applications. thesis no 579. Tech. rep., Linköping University, Linköping Studies in Science and Technology. Doctoral dissertation.
- [5] Bishop, C. M., 2006. *Pattern Recognition and Machine Learning*. Springer.
- [6] Bou-Ammar, H., Voos, H., Ertel, W., Sept 2010. Controller design for quadrotor uavs using reinforcement learning. In: *International Conference on Control Applications*. pp. 2130–2135.
- [7] Busoniu, L., Ernst, D., Schutter, B. D., Babuska, R., April 2011. Approximate reinforcement learning: An overview. In: *Symposium on Adaptive Dynamic Programming and Reinforcement Learning (ADPRL)*. pp. 1–8.
- [8] Calinon, S., D'halluin, F., Sauser, E. L., Caldwell, D. G., Billard, A. G., June 2010. Learning and reproduction of gestures by imitation. *IEEE Robotics Automation Magazine* 17 (2), 44–54.
- [9] Chambrion, G. d., Billard, A., 2014. Learning search policies from humans in a partially observable context. *Journal of Robotics and Biomimetics* 1 (1), 1–16.
- [10] Cheng, H., Chen, H., May 2014. Online parameter optimization in robotic force controlled assembly processes. In: *International Conference on Robotics and Automation (ICRA)*. pp. 3465–3470.
- [11] Cheng, H., Chen, H., Hao, L., Li, W., May 2014. Robot learning based on partial observable markov decision process in unstructured environment. In: *International Conference on Robotics and Automation (ICRA)*. pp. 4399–4404.
- [12] Chhatpar, S. R., Branicky, M. S., 2001. Search strategies for peg-in-hole assemblies with position uncertainty. In: *International Conference on Intelligent Robots and Systems (IROS)*. Vol. 3. pp. 1465–1470.
- [13] Deisenroth, M. P., Neumann, G., Peters, J., 2011. A survey on policy search for robotics. *Foundations and Trends in Robotics* 2 (1-2), 1–142.
- [14] Ernst, D., Geurts, P., Wehenkel, L., April 2005. Tree-based batch mode reinforcement learning. *Journal of Machine Learning Research* 6, 503–556.
- [15] Gordon, G. J., 1995. Stable function approximation in dynamic programming. In: *International Conference on Machine Learning (ICML)*. pp. 261–268.
- [16] Grondman, I., Busoniu, L., Lopes, G. A. D., Babuska, R., Nov 2012. A survey of actor-critic reinforcement learning: Standard and natural policy gradients. *IEEE Transactions on Systems, Man, and Cybernetics, Part C (Applications and Reviews)* 42 (6), 1291–1307.
- [17] Gullapalli, V., Barto, A. G., Grupen, R. A., 1994. Learning admittance mappings for force-guided assembly. In: *International Conference on Robotics and Automation (ICRA)*. pp. 2633–2638.
- [18] Hausknecht, M., Stone, P., 2015. Deep recurrent q-learning for partially observable mdps. *CoRR*.
- [19] Kalakrishnan, M., Righetti, L., Pastor, P., Schaal, S., Sept 2011. Learning force control policies for compliant manipulation. In: *International Conference on Intelligent Robots and Systems (IROS)*. pp. 4639–4644.
- [20] Kronander, K., 2015. Control and learning of compliant manipulation skills.
- [21] Lange, S., Riedmiller, M., July 2010. Deep auto-encoder neural networks in reinforcement learning. In: *The 2010 International Joint Conference on Neural Networks (IJCNN)*. pp. 1–8.
- [22] Lauri, M., Ritala, R., 2016. Planning for robotic exploration based on forward simulation. *Robotics and Autonomous Systems*.
- [23] Meeussen, W., et. al, May 2010. Autonomous door opening and plugging in with a personal robot. In: *International Conference on Robotics and Automation (ICRA)*. pp. 729–736.
- [24] Mnih, V., et. al, feb 2015. Human-level control through deep reinforcement learning. *Nature* 518, 529–533.
- [25] Nemec, B., Abu-Dakka, F. J., Ridge, B., Ude, A., Jorgensen, J. A., Savarimuthu, T. R., Jouffroy, J., Petersen, H. G., Krüger, N., Nov 2013. Transfer of assembly operations to new workpiece poses by adaptation to the desired force profile. In: *International Conference on Advanced Robotics*. pp. 1–7.
- [26] Neumann, G., Peters, J., Jun. 2009. Fitted q-iteration by advantage weighted regression. In: *Advances in neural information processing systems (NIPS)*. Vol. 21. pp. 1177–1184.
- [27] Neumann, G., Peters, J. R., 2009. Fitted q-iteration by advantage weighted regression. In: Koller, D., Schuurmans, D., Bengio, Y., Bottou, L. (Eds.), *Advances in Neural Information Processing Systems (NIPS)*. Vol. 21. Curran Associates, Inc., pp. 1177–1184.
- [28]Ormoneit, D., Glynn, P., Oct 2002. Kernel-based reinforcement learning in average-cost problems. *IEEE Transactions on Automatic Control* 47 (10), 1624–1636.
- [29] Peters, J., Schaal, S., 2008. Natural actor-critic. *European Symposium on Artificial Neural Networks* 71 (7-9), 1180–1190.
- [30] Peters, J., Schaal, S., 2008. Natural actor-critic. *Neurocomputing* 71 (7-9), 1180–1190.
- [31] Pineau, J., Gordon, G., Thrun, S., August 2003. Point-based value iteration: An anytime algorithm for pomdps. In: *International Joint Conference on Artificial Intelligence (IJCAI)*. pp. 1025–1032.
- [32] Riedmiller, M., 2005. *Neural Fitted Q Iteration - First Experiences with a Data Efficient Neural Reinforcement Learning Method*. Vol. 16. Springer

- Berlin Heidelberg, pp. 317–328.
- [33] Schaal, S., Peters, J., Nakanishi, J., Ijspeert, A., 2004. Learning movement primitives. In: International Symposium on Robotics Research (ISRR).
 - [34] Sung, H., 2004. Gaussian mixture regression and classification. Ph.D. thesis, Rice University.
 - [35] Sutton, R., Barto, A., 1998. Reinforcement learning: An introduction. Vol. 116. Cambridge Univ Press.
 - [36] Vien, N. A., Toussaint, M., Sept 2015. Pomdp manipulation via trajectory optimization. In: International Conference on Intelligent Robots and Systems (IROS). pp. 242–249.
 - [37] Wiering, M., van Otterlo, M., 2012. Reinforcement Learning State-of-the-Art. Springer-Verlag Berlin Heidelberg.
 - [38] Yang, Y., et al., 2014. Fast programming of peg-in-hole actions by human demonstration. pp. 990–995.